MeV proton acceleration at kHz repetition rate from ultra-intense laser liquid interaction

To cite this article before publication: John T Morrison *et al* 2018 *New J. Phys.* in press https://doi.org/10.1088/1367-2630/aaa8d1

MeV proton acceleration at kHz repetition rate from ultra-intense laser liquid interaction

John T. Morrison
Innovative Scientific Solutions, Inc., Dayton, OH, 45459, USA

Scott Feister
University of Chicago, Chicago, IL, 60637, USA

Kyle D. Frische
Innovative Scientific Solutions, Inc., Dayton, OH, 45459, USA

Drake R. Austin
Department of Physics, The Ohio State University, Columbus, OH, 43210, USA

Gregory K. Ngirmang
Department of Physics, The Ohio State University, Columbus, OH, 43210, USA
Innovative Scientific Solutions, Inc., Dayton, OH, 45459, USA

Neil R. Murphy
Air Force Research Laboratory Materials and Manufacturing Directorate, WPAFB, OH, 45433, USA

Chris Orban
Department of Physics, The Ohio State University, Columbus, OH, 43210, USA

Enam A. Chowdhury
Department of Physics, The Ohio State University, Columbus, OH, 43210, USA
Intense Energy Solutions, LLC., Plain City, OH, 43064, USA

W. M. Roquemore
Air Force Research Laboratory, WPAFB, OH, 45433, USA

Abstract. Laser acceleration of ions to $\gtrsim$MeV energies has been achieved on a variety of Petawatt laser systems, raising the prospect of ion beam applications using compact ultra-intense laser technology. However, translation from proof-of-concept laser experiment into real-world application requires MeV-scale ion energies *and* an appreciable repetition rate (>Hz). We demonstrate, for the first time, proton acceleration up to 2 MeV energies at a kHz repetition rate using a milli-joule-class short-pulse laser system. In these experiments, 5 mJ of ultrashort-pulse laser energy is delivered at an intensity near $5 \cdot 10^{18}$ W cm^{-2} onto a thin-sheet, liquid-density target. Key to this effort is a flowing liquid ethylene glycol target formed in vacuum with thicknesses down to 400 nm and full recovery at 70 μs, suggesting its potential use at $\gg$kHz rate. Novel detectors and experimental methods tailored to high-repetition-rate ion acceleration by lasers were essential to this study and are described. In addition, Particle-in-cell simulations of the laser plasma interaction show good agreement with experimental observations.

PACS numbers: 00.00, 20.00, 42.10

Keywords: Ion Acceleration, IOP journals Submitted to: *New J. Phys.*

1. Introduction

Since the demonstration of ultra-intense-laser-generated MeV protons from the Nova Petawatt laser system [1], ion acceleration from laser-plasma interactions (LPI) with solid-density targets has been a subject of particular interest for the field of ultra-intense-laser science. This interest is from a fundamental perspective in ultra-intense laser plasma interaction (ULPI), the time-resolved probing of ULPI [2], and the isochoric heating of targets [3, 4] into a state of warm dense matter (WDM). Laser-driven ion acceleration is also interesting for the prospect of developing novel, compact and cost-effective ion sources for a variety of uses: cancer radiotherapy [5, 6, 7], short-lived medical isotope production for positron emission tomography (PET) [8, 9], secondary neutron generation [10, 11, 12, 13, 14], surface engineering [15], material processing [15], and others [16]. Each of these potential applications of ultra-intense laser plasma technology will require ion acceleration to occur at simultaneously relevant energies, fluence, and repetition rate.

The most well known and well studied mechanism for accelerating ions via ultra-intense laser matter interactions is target normal sheath acceleration (TNSA) [17], or collisionless plasma expansion [18, 19, 20]. Energetic electrons produced from LPI propagate through a micron-scale solid-density target. A small percentage of electrons escape the target and leave behind positively charged ions, and remaining energized electrons create and become trapped by an electrostatic "sheath" field at the target-vacuum interface. This sheath field is typically strong enough to significantly affect the energies of subsequent MeV electrons escaping the target region [21]. The sheath field

accelerates protons and carbon ions from the contaminant layer on the surface of the target in the direction perpendicular to the target plane [22, 12]. Other mechanisms for accelerating ions exist [23], such as relativistic light sail [24], radiation pressure acceleration (RPA) [25] and break out afterburner (BOA) [26, 27]. These mechanisms can accelerate a volume of ions from an ultra-thin (tens of nanometers thick) target, potentially with a higher efficiency and a higher cutoff energy than can achieved by TNSA. These ion acceleration schemes typically require large laser facilities that produce many Joules-per-shot laser pulses. Unfortunately, due to present limitations on the time-averaged power of ultra-intense laser systems, these novel mechanisms can only be sustained with a repetition rate of order one shot per minute [28].

Current limitations of LPI repetition-rate pose significant problems for the translation of proof-of-concept laser experiments into real-world applications [29]. To address the issue, recent efforts are moving both lasers [30] and targets [31] used in ion acceleration toward repetition rates of order a Hz [32, 33]. Of particular difficulty is designing a system that can simultaneously operate at a high repetition rate and a sufficiently low ambient pressure, and that quickly refreshes to the approximately the same target within sub-micron tolerances such that the laser interaction remains at peak focus. Moreover, the target choice needs to avoid or suppress build-up of debris on optical elements in the target chamber to facilitate continuous use for extended periods of time. Typically, laser-based ion acceleration uses high laser intensities, thin targets, low background pressure, and near-solid target densities.

Liquid targets have a number of attractive features for meeting these needs. Liquid targets can be rapidly delivered into the interaction region, and mitigate debris [34, 35, 36, 31]. Previous efforts to accelerate ions using liquid targets have yielded ion energies well below an MeV, although it should be noted that Ref. [37] used an ultra-short laser pulse to prompt neutron-producing D-D reactions at a 0.5 kHz repetition rate using a ~ 10 μm diameter cylindrical flowing liquid (D_2O) target. The goal of that experiment was to demonstrate production of in situ neutrons, rather than accelerate ions out of the target to MeV energies. Another recent work [38] uses a solid hydrogen column target with a 150 TW (multi-Joule) laser to generate multi-MeV protons. This target has potential for high-repetition-rate operation using a cryogenic setup in high vacuum.

In the experiment reported here, a versatile, room-temperature, and planar liquid target is shown to accelerate MeV protons at an unprecedented kHz repetition rate in a 'low vacuum' environment. This work opens the door for worldwide use of ultrafast MeV protons as experimental, diagnostic, and materials research tools for myriads of small laser labs with access to few-mJ ultrafast lasers. Three developmental aspects were crucial to obtaining kHz ion acceleration: design of a kHz-capable flowing thin-film target, innovation of high-repetition-rate ion spectral diagnostics, and implementation of a chamber pressure environment capable of simultaneously sustaining liquid targets *and* ion acceleration. We report here the acceleration of up to 2 MeV protons at a kHz repetition rate with a sub-TW milli-joule laser system.

2. Experimental Setup

The experimental setup is shown in Fig. 1, where a dual multi-pass amplifier Ti:Sapphire kHz laser system (KMLabs Red Dragon system, heavily modified for energy, mode and contrast improvements) delivers up to 11 mJ pulses at 780 nm with 40 fs pulse duration (FWHM) into a vacuum target chamber [39, 40, 41] where it can be focused onto the liquid sheet target. In the experiment described here, the laser system delivered 8 mJ pulses into the target chamber. The picosecond-timescale pulse contrast of the laser pulses is measured to be at the 10^{-6} level ($\pm$100 ps) and the nanosecond-timescale contrast level is approximately 10^{-10} beyond -6 ns due to extinction from an external Pockels cell and polarizer setup. The final focusing element is a 45° angle of incidence F/1 protected gold coated off axis parabola (OAP) with a Strehl ratio > 0.97 (Aperture Optical Sciences) which produces a 1.8 μm laser focus (FWHM). Accounting for the distribution of pulse energy in time from our ns to ps pulse contrast measurements, distribution of energy in the focal spot measured to 1 part in 10,000 and the losses in optical elements, we estimate that approximately 5 mJ short-pulse laser energy/pulse was delivered onto the target within 99% of Gaussian intensity profile of the focus.

We produce thin liquid sheets through an off-center collision of two liquid jets [42, 43]. At the heart of the liquid sheet target system is a high pressure syringe pump (Isco, Model 100DX) capable of producing a constant flow at 10,000 PSI. A continuous supply of liquid is fed into the pump from a reservoir. The liquid is then transported under high pressure to the target chamber via 1/16 inch stainless steel (SS) tubing and compression fittings via a vacuum feed-through. The liquid delivery SS tubing line is attached to a precision alignment system inside the vacuum chamber. The tube then splits into two separate lines ending in equal length, 25 micron diameter capillaries. A manual adjustable valve controls the flow of liquid into the second line. One of the SS liquid lines is attached to a nano-positioning piezoelement-driven xyz translation stage, so that it can be positioned with precision with respect to the other liquid line. This target assembly is mounted on a rotation stage, which is mounted on an xyz precision micro-positioning stage. This allows the whole assembly and target to translate and rotate around the vertical axis as seen in Fig. 1(b), allowing control of the polar angle of incidence of the liquid sheet with the laser.

When the pump is operating near 8500 PSI, the 24 m/s colliding streams produce a sub-micron thick sheet of liquid (Fig. 1(b)) moving at 16 m/s. The target and crucially the LPI affected region of the target moves 16 mm between kHz pulses, ensuring an unperturbed sheet for each shot. For this experiment, the angle between the two input streams is 60° (see Fig. 1(b)). The sheet forms in a plane rotated from the plane of the streams by 15° (see Fig 1(a)); this can be adjusted by horizontal overlap of the stream cross-sections. The thickness of the sheet is measured in situ using a commercial interferometric thin film measurement instrument (Filmetrics). Using a series of shadowgraphic images of the target interaction, similar to those in Fig. 5, the standard deviation of the target position is restricted to be between 0.6 and 2.0

microns. Turbulent behavior is not observed in the stream collision or the sheet, and one can infer surface tension dominated laminar flow. Various liquids can be used in this system, including water, methanol, and other organic solvents. In this experiment, we use ethylene glycol to achieve lower background pressure in the chamber.

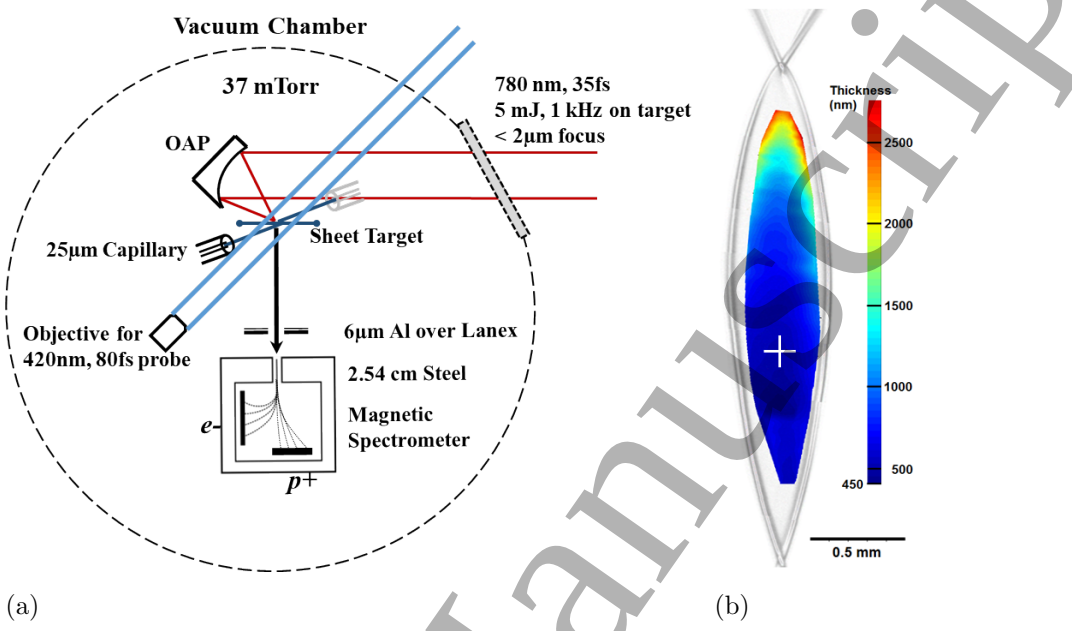

Figure 1. (a) Schematic of 1 kHz rep-rate LPI with a thin, free-standing, sub-micron liquid target. Primary diagnostic is a magnetic spectrometer collecting both e- and p+ spectra at target normal. Lanex covered with 6 μm Al imaged on a camera (not shown) is used to optimize alignment in situ. Line CCDs with a 508 μm coating of RP-408 scintillating plastic allows for 100 Hz acquisition. To remove scatter, the electron and proton detectors have 6 μm and 60 nm Al respectively. (b) Shadowgraph (gray) and thickness (pseudo-color) of a stable, free-standing, sub-micron liquid target created from two 30 μm impinging jets. The thickness was measured by imaging 25 micron patches of transmitted white light into a commercial interferometric thin film measurement unit (Filmetrics). The 550 nm thick interaction location is indicated by a white cross.

An important feature to the design of the liquid target system is the extraction of liquid from the target chamber, without which the liquid evaporates inside the chamber. This can reduce or negate ion acceleration by raising the chamber pressure. The drainage system consists of an extraction pipe directly underneath the capillary streams, which takes the liquid out of the main target chamber to a separate collection chamber outside of the main chamber. This collection chamber, with liquid accumulating at the bottom, is continuously evacuated by a small turbo pump. A conical metal catcher with a central hole is positioned on top of the extraction pipe opening to reduce backstreaming of liquid vapor back into the main chamber from the liquid collection chamber. Arranging for the liquid to collide with the drainage system at grazing incidence dramatically reduces the amount of vaporization. This system allows the background pressure to be stabilized ~20 mTorr, and ~40 mTorr with laser pulses hitting the target at kHz rate.

The target position is precision controlled via piezo-actuator based stages and is monitored in situ via a 420 nm femtosecond probe pulse using synchronous shadowgraphy and interferometry described in detail elsewhere [44]. This system allows observations of the laser target interaction with micron spatial and 80 fs temporal resolution with an arbitrary (ms to ps) delay line. For our ion acceleration experiments, the target was rotated so that the high intensity laser pulses are incident on target at 45° angle with p-polarization. Real time confirmation of particle emission angle is provided by monitoring electrons using a Lanex screen imaged onto a CCD camera. This Lanex screen, covered with 6 μm of Al, has a hole in its center along the line of sight of a custom-built particle spectrometer.

The particle spectrometer entrance slit was positioned normal to the target at a distance of 130 mm to collect accelerated electrons and ions ejected from the target simultaneously. The particle spectrometer is compact and well-shielded. Rare earth magnets provide a 0.13 T magnetic field that is energy calibrated for both electrons and ions via 3D field measurement and simulations, and experimentally with mono energetic MeV electron beams from an accelerator [41]. Both electron and ion detectors are Linear CCDs with 508 μm of RP408 plastic scintillator bonded with index-matching epoxy. The electron and ion detectors are covered with 6 μm Al foil and 60 nm of Al deposition [45] respectively to block scattered light. We operate the linear CCDs at the maximum 100 Hz acquisition rate, with synchronized sub-ms exposure time to capture one out of ten shots during kHz laser operation. We note that there exists commercially available CCDs that would allow acquisition rates at or above 1 kHz. Particles enter the spectrometer through a 1.0 x 1.2 mm slit entrance (subtending $3.8 \cdot 10^{-5}$ s.r.) set in 29 mm thick stainless steel. Fig. 4 presents spectra both with and without the effect of the slit deconvolved from the data. The sensitivity of the RP408-covered CCDs was calculated for each energy by first modeling the energy deposited as a function of depth using the stopping and range of ions in matter (SRIM) code [46]. The contribution for each depth in the scintillator is reduced by attenuation of the plastic and geometric collection in the CCD assuming the scintillation is isotropic. Finally, sensitivity is calculated using the spectral sensitivity of the CCD, emission spectra and scintillation efficiency of the scintillator. To confirm the particle type and corroborate the calculated sensitivity of the RP408-covered CCDs, CR39 particle track detectors were employed. The CR39 detectors can be used in place of the RP408-attached CCD array ion detector inside the particle spectrometer, while the electron CCD detector remains in place and can continue providing electron data. For the CR39 irradiation, the electron signal was optimized (corresponding to a 0 μm target focal position in Fig. 3) with 3mJ on target and a peak intensity of $8 \cdot 10^{18}$ W/cm^2. During the experiment, as the CR39 detectors were irradiated with ions, and MeV electron signals were monitored as before to indicate consistent conditions for the two proton detectors. Layers of 1.5 micron Mylar sheets were placed on CR-39 sheets with a stair-case profile to confirm that the $\gtrsim$MeV proton signal can penetrate an appropriate number of layers and still leave behind damage tracks observed as pits in the developed CR-39 sheets.

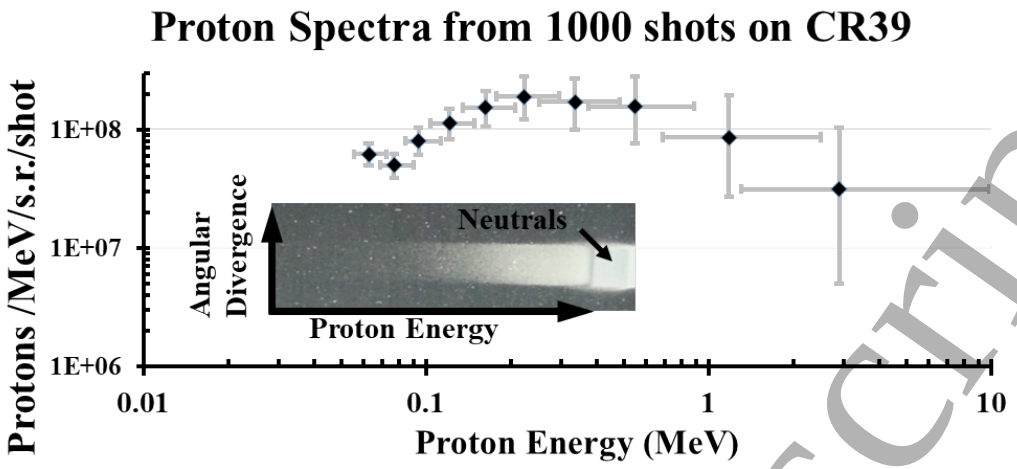

Figure 2. Integrated proton spectra from 1000 shots for the target at focus using a CR39 plastic detector in place of a CCD detector in the particle spectrometer. Inset: Raw CR39 data from the particle spectrometer.

During the particular run the CR39 data used for the absolute proton yield measurement shown in Fig. 2 was collected, the ion signal was captured from 1000 shots (accumulation of 100 seconds of 10Hz operation) and no Mylar film was used. After etching, particle tracks were counted using a digital scanner and counting all individual pits.

3. Results

The single-shot ion and electron spectra of Fig. 3, both experimentally recorded in less than few minutes, are the primary result of this paper. As laser focal depth is varied, intensity on the target of the main pulse and pre-pulses is modified. The results show $\gtrsim$MeV ion acceleration at 1 kHz and both plots demonstrate the experimental versatility of a high-repetition-rate data acquisition system coupled with liquid-sheet targets.

The combination of kHz laser, target, and a high repetition rate data acquisition system enables us to optimize proton/electron signal intensity and energy in real-time as functions of various experimental parameters. A typical optimization procedure utilizes the shadowgraph of the LPI *itself* (as in Fig. 5) to choose an approximate target transverse position and focal depth. We then rotate the target to aim the energetic electrons accelerated from the back of the target to the Lanex screen positioned around the entrance slit of the particle spectrometer (crude optimization). We further optimize for high-energy ions in the spectrometer by iterating between target angle and focal depth to finalize the target angle. This optimization is performed once, prior to focal scan. The data for the focal scan in Fig. 3 can be generated by simply choosing to store the data from the electron and ion spectrometers while translating the target at a fixed rate, here 1 μm/s steps, though various target positions.

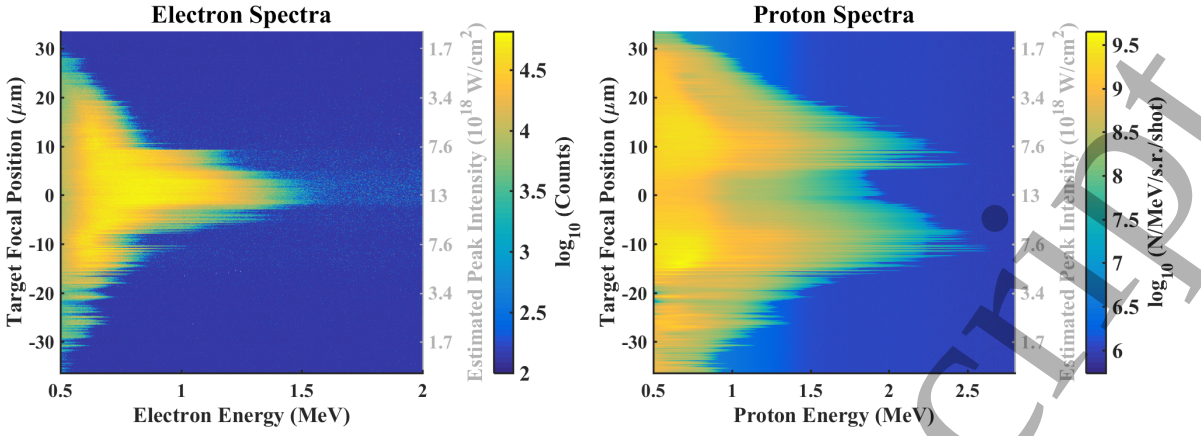

(a) (b)

Figure 3. Single shot, target normal, experimental electron (a) and ion (b) spectra as a function of focal position of the liquid target (Fig. 1(b)). The spectra are acquired simultaneously while moving the target in 1 μm steps along the laser propagation direction. The quenching of the ion acceleration and enhancement of the electron spectra is consistent with the introduction of a pre-plasma at higher intensities closer to focus (see Fig. 5). Here, positive focal distances represent laser focus in front of the target (diverging beam hitting the target).

As one expects, the number, characteristic temperature and cut-off energy of both electron and proton spectra increase as the target is closer to best focus [47] where the peak intensity increases to $1.3 \cdot 10^{19}$ W cm^{-2}. Notably, the electron signal sharply increases and the proton signal drops for focal positions near $z = 0$ (see Discussion for explanation). For the scan presented here, the energetic ion spectra are observed for target positions $z \approx \pm 10$ μm. The most energetic spectra at $z = -12$ μm have characteristic temperatures 450 ± 20 keV and cut-off energies of 2.3 ± 0.2 MeV. At this position, the peak intensity is measured to be $5 \cdot 10^{18}$ W cm^{-2} and the estimated laser-to-proton conversion efficiency is $\sim 0.5\%$ assuming the ions expand in a cone with a half-angle of 10° consistent with previously reported data [48] and the PIC simulation as seen in the bottom right panel of Fig. 4.

We have demonstrated a target and method for high-repetition-rate laser based ion acceleration. Fig. 3(b) shows that the ion acceleration is effective not just on average but on a shot-to-shot basis, demonstrated here at 1 kHz. Two colliding liquid streams are used to generate a continuously refreshing sub-micron, solid density target(Fig. 1(b)). Using this target we have shown measurement and optimization of MeV ion acceleration at a kHz repetition rate, with 100 Hz single-shot acquisitions. We have provided a clear method for optimization and experimental alignment through real-time feedback.

3.1. Simulation

We performed a simulation to show the best case for the proton cutoff energy with our chosen target and thickness given no pre-plasma. We performed a 2D($3v$) Particle-in-

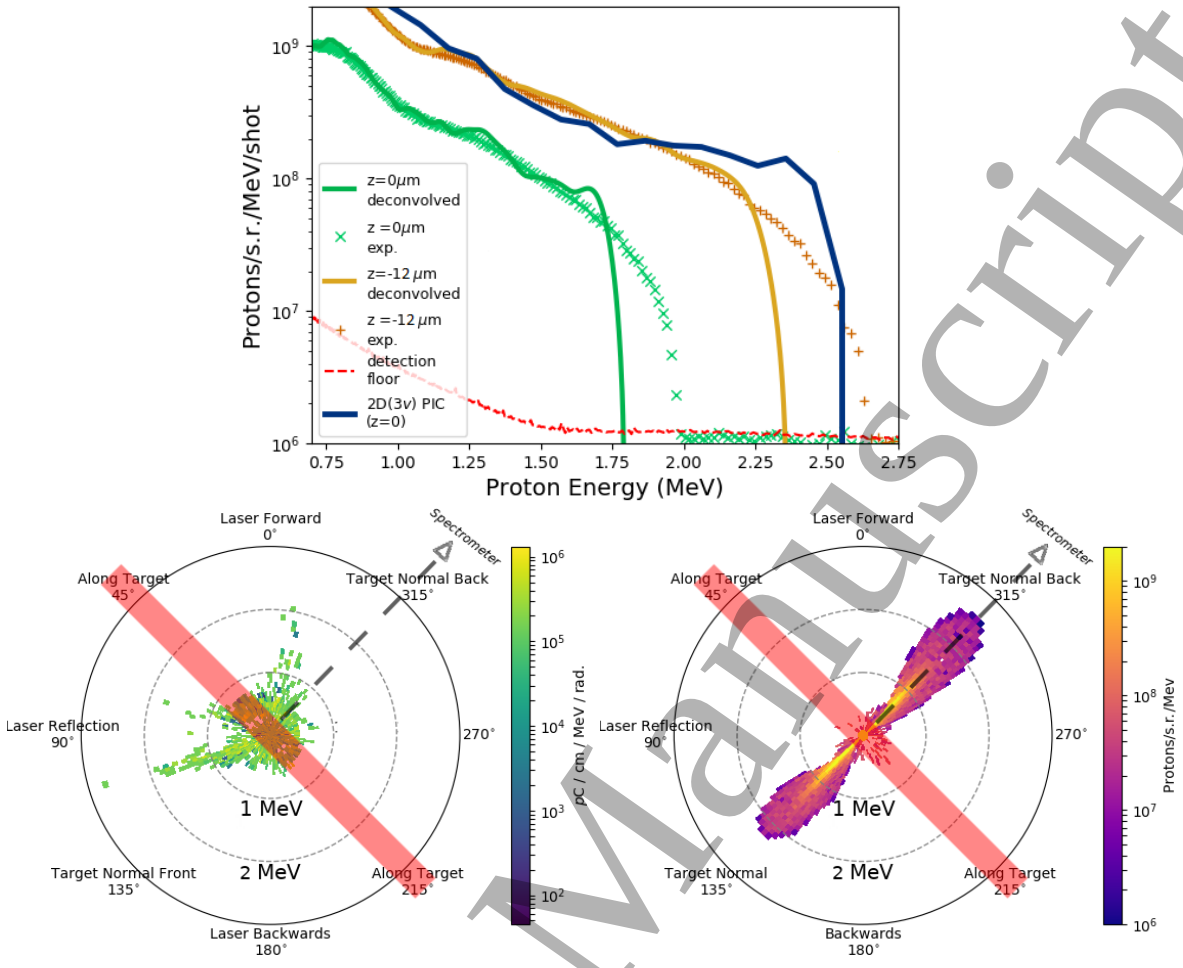

Figure 4. Top: Spectra of protons from select shots chosen based on the location of the laser focus (orange crosses, 12 μm in front of target; green x's, target center; solid green and orange, after slit width deconvolved), and the PIC simulation spectra in a 5 μm wide box normal to the target (blue). The detection floor is plotted in the dashed, red line. Bottom Left: Energy and angular spectra of escaping electrons from the PIC simulation. The position of a bin around the circle corresponds to the escaping momentum angle for an electron that escapes the simulation, while the distance from the center corresponds to energy of the bin. The angles along the target are highlighted in red while a dotted line shows the angle from which the spectrometer in the real experiment would observe. Bottom Right: Energy and angular spectra of escaping protons from the PIC simulation scaled to match the empirical target normal yield measurement.

Cell (PIC) simulation with the Large-Scale Plasma (LSP) code [49, 50] to model the acceleration of protons using a $5 \cdot 10^{18}$ W/cm^2 peak intensity laser pulse incident on a ethylene glycol target at 45°. The incident laser is treated as a spatially Gaussian pulse with a Gaussian radius of 1.87 μm and temporally sine-squared pulse with a temporal FWHM of 42 fs. The simulation space was a 28 μm by 28 μm simulation box with a 25 μm wide target with a thickness of 460 nm. The reduced size of the target (25 μm)

was chosen in order to minimize computational cost. The target was initialized with all ions singly ionized (C^+,O^+,H^+) and in proportion to the chemical composition of ethylene glycol, whose ionization potential (IP) is 10.16 eV. It should be noted that IP of C^+,O^+,H^+ are approximately 11, 13.6 and 13.6 eV respectively and therefore, it is entirely justified to assume glycol to be in a dissociated state and its constituent atoms singly ionized by prepulse or the the rising edge of the main pulse [51], at intensities 10^{13} - 10^{14} W/cm^2, at least 100s of femtoseconds before the arrival of the peak of the pulse (for progressive optical field ionization of a single species between 10^{13} - 10^{18} W/cm^2, see [52]). Electrons were present to maintain charge neutrality at the start of the simulation. From the mass density of liquid glycol with singly ionized ions, an initial electron number density of 10^{23} cm^{-3} was assumed. Initial temperatures for all species were set to 1 eV, which may or may not be hotter than the actual target due possible laser pre-pulse effects that we do not model. But, importantly, a temperature of 1 eV is a small enough temperature that the target ions exhibit negligible movement before the ultra-intense pulse reaches the target. The simulations employed a spatial resolution of 10 nm, with 9 particles per cell per species initially. The code includes an ionization model consistent with the ADK/PPT rate [53, 54] which can increase the electron particle count as the laser propagates through the simulation. Our simulation does not resolve the Debye length, however, instead we employ an implicit field solver that minimizes numerical heating, allowing us to have cell sizes that somewhat exceed the debye length. It is important to note that the simulated laser pulse was configured so that the peak focus was directly on the target ($z = 0$), rather than being $\sim$10 μm ahead or behind the target ($z = \pm 10$ μm), which Fig. 3 indicates was optimal for proton acceleration, which will be discussed in the next section.

The energy spectrum of protons 873 fs after the tail of the pulse has left the target is displayed alongside experimental data for two different focal positions on the top graphic in Fig. 4. As can be seen, the simulated proton spectrum extends to 2.5 MeV followed by a sharp drop off in energy, a signature of the TNSA mechanism which is in fair agreement with the experimentally-measured cutoff. The simulated proton angular and energy spectra are shown in Fig. 4 bottom right. According to the simulation, the electric field just after the laser has left the simulation space indicates a sheath field around 0.8 TV/m, similar to expectations for TNSA with a PW class laser (e.g. [55]). It is also worth mentioning that the number of protons and the cut-off should exceed the experimentally observed targets by a small factor given the lower dimensionality of the 2D($3v$) simulation and the fact that we do not include effects due to laser pre-pulse in our simulations, which would be important especially when the laser focus is on target.

Fig. 4 bottom left plot displays the angular and energy spectrum of electrons that have escaped the simulation after 873 fs. It shows that the highest energy electrons emerging from the back of the target is aligned close to the laser axis, thereby missing the particle spectrometer, which is aligned normal to the target. The electron cutoff along that direction predicted by the simulation is in very good agreement with experimental electron spectra shown in Fig. 3(a).

4. Discussion

Figs. 3(b) present direct measurements of proton acceleration to 2 MeV from a sub-TW millijoule class laser system operating at a kHz repetition rate (5 mJ of short pulse energy on target). The system and its methods have avenues to scaling in proton energy and repetition rate. Utilizing shadowgraphy as in Figure 5 with μs probe delays, one can observe the interaction region move as it evolves with the initial fluid velocity (conservation of momentum). After 16 μs, the $\sim$ 350 μm extent of the LPI perturbation in the fluid leaves the focal position. There is $\sim$ 50 μm of undisturbed target around the focal position after 20 μs and the film is entirely refreshed after in 70 μs. Using these recovery times, we estimate that the target described here can support 50 kHz repetition rates, and would support repetition rates $>$ 10 kHz from Joule-class laser systems provided effects of the LPI do not propagate up the streams before they collide. We have provided a self-refreshing target with a clear path to higher rep-rate, higher energy and higher fluence proton beams.

Simulations and experimental shadowgraphy indicate that the current system has the potential for increased proton yields and energies through improvement of the laser contrast characteristics. Fig. 3 indicates that the best proton acceleration results were obtained when the laser focus was placed at $z \approx \pm 10$ μm from the target. One might expect that the best ion acceleration would occur at peak focus ($z = 0$) because this provides the highest on-target intensity [56]. The key to understanding this result, however, is to appreciate that this is true for both the main pulse, and the pre-pulse which can affect the target in the nanoseconds-to-picoseconds before the arrival of the ultra-intense pulse. In the experiment there is a 10^{-6} contrast replica of the main pulse that occurs 6.1 ns before the main pulse interaction. This pre-pulse feature can be removed in future experiments by further modification of the laser system [57]. If pre-pulse perturbs the back surface of the target, the TNSA process will be stifled [48]. Higher pre-plasma conditions that shut down the TNSA process also would contribute to more energetic electron acceleration [58].

Fig. 5 provides clear evidence that the effect of the 10^{-6} contrast short-pulse replica on the liquid sheet target is much more pronounced when the laser is configured at peak focus than when it is 10 microns away from peak focus ($z \approx 10$ μm). This can be seen especially with the panels of Fig. 5 that highlight the condition of the target at 1.47 ps before the arrival of the main pulse. It appears that at $z \approx 10$ μm, much of the short pulse replica is simply transmitted through the target, leaving only a subtle impression at 1.47 ps, whereas at peak focus ($z = 0$) the effect on the target is more substantial.

With the shadowgraphy results presented in Fig. 5, the results of Fig. 3, which show lower peak proton energy for peak focus conditions, can be attributed to the pre-pulse at-least-partially punching through the target. This interpretation is also corroborated by the electron spectra, which becomes much more energetic at peak focus as one would expect if the target density in the interaction region is decreased to near or less-than critical density due to the short-pulse replica interaction [59].

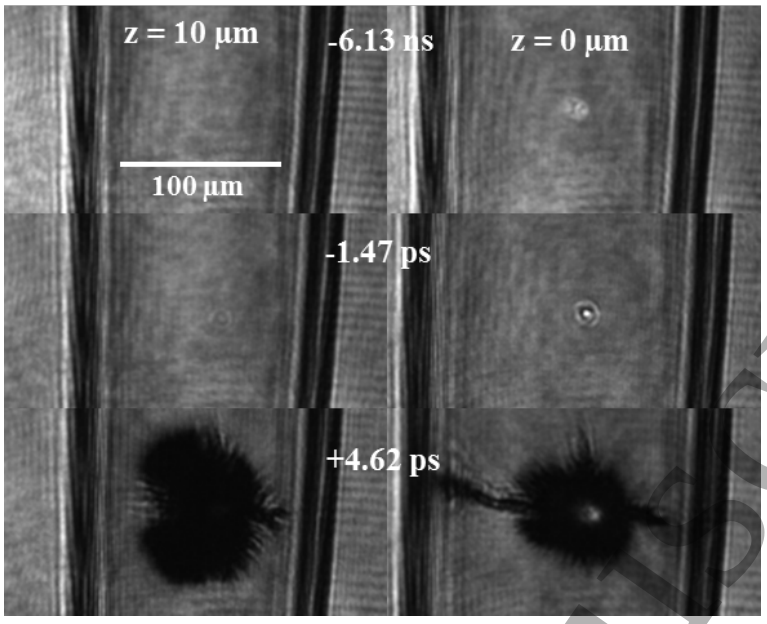

Figure 5. Shadowgraphy of the laser plasma interaction illuminated by an 80 fs probe at three different delays to the pump laser for two different target positions. The target 10 μm from focus (left) remains unperturbed until -1.47 ps before main pulse, and has stronger proton acceleration, and less energetic escaping electrons. The target at focus (right) is perturbed -6.13 ns before the main pulse interaction from which more numerous and energetic electrons escape, and the ion acceleration is suppressed.

It is clear from Figs. 3(b) and 5, that pulse contrast improvement of our laser system (which is under way) would allow for the peak intensity to interact with an unperturbed target resulting in significant increase of the proton cutoff energy [7]. A more recent review article [51] discusses proton cutoff energy vs laser pulse energy and shows from existing data of laser proton experiments that at least 100 mJ energy/pulse would be required to reach 1 MeV proton energy. With tight focusing and precision target positioning, we seem to have lowered that technological threshold. With higher contrast pulses allowing the use of thinner targets (our system is capable of producing 150 nm thick targets), in combination with more energy/pulse (e.g. $\sim$ 50 mJ/pulse), a system could produce 10 MeV or higher energy protons. From an applications perspective, when proton energies exceed 3 MeV, the proton beam can propagate significant distances in air without experiencing much loss, which would open up pathways to PIXE and proton bombardment materials research without need to manipulate samples and detectors in vacuum. It would also make it easy to probe live biological systems with ultra-fast proton beams for diffraction and radiography applications.

For application, absolute proton yield of a source is as important as its energy characteristics. From that perspective, how well does our laser proton source compare with more traditional joule class laser proton sources? As an example, when compared with absolute numbers from proton acceleration experiments carried out by a 100 TW laser system with nanostructured foils [60] enhancing proton numbers 5 times that

from simple foils, at 2 MeV, our absolute yield/MeV-sr-shot is lower by three orders of magnitude. However, at kHz repetition rate, our proton production rate per second would be on par with a 100 TW proton acceleration system with non-simple targets operating at 1 Hz, which, we believe, would be technologically far more challenging.

5. Conclusion

We have demonstrated up to ∼2 MeV proton acceleration from a sub-TW millijoule class laser system operating at a kHz repetition rate. These results were obtained with 8 mJ of laser energy entering the target chamber and 5 mJ of ultrashort pulse energy reaching the target, interacting at a peak intensity near $5 \cdot 10^{18}$ W cm^{-2}. Importantly, this ion energy is within an order of magnitude of experiments performed with much lower repetition rate with Petawatt-class laser systems (e.g. [1, 31]). Key to the success of this experiment is a liquid sheet target system that we describe which continuously produces highly-controlled sub-micron sheet targets using ethylene glycol to achieve low background pressure. High acquisition rate, real-time data analysis also played an important role in finding optimal conditions for proton acceleration. The success of this experiment is significant for the wider effort to deliver a variety of real-world applications of compact ultra-intense laser technology, all of which rely upon creating relativistic laser interactions with appreciable repetition rates.

6. Acknowledgement

This research is supported by the Air Force Office of Scientific Research under LRIR Project 17RQCOR504 under the management of Dr. Riq Parra and Dr. Jean-Luc Cambier. This project also benefited from a grant of time at the Garnet supercomputer (ERDC) and storage space at the Ohio Supercomputer Center. Support was also provided by the DOD HPCMP Internship Program and the AFOSR summer faculty program.

References

[1] Snavely R A, Key M H, Hatchett S P, Cowan T E, Roth M, Phillips T W, Stoyer M A, Henry E A, Sangster T C, Singh M S, Wilks S C, MacKinnon A, Offenberger A, Pennington D M, Yasuike K, Langdon A B, Lasinski B F, Johnson J, Perry M D and Campbell E M 2000 *Phy. Rev. Lett.* **85**

[2] Mackinnon A J, Patel P K, Town R P, Edwards M J, Phillips T, Lerner S C, Price D W, Hicks D, Key M H, Hatchett S, Wilks S C, Borghesi M, Romagnani L, Kar S, Toncian T, Pretzler G, Willi O, Koenig M, Martinolli E, Lepape S, Benuzzi-Mounaix A, Audebert P, Gauthier J C, King J, Snavely R, Freeman R R and Boehlly T 2004 *Review of Scientific Instruments* **75** 3531–3536 ISSN 00346748

[3] Patel P, Mackinnon A, Key M, Cowan T, Foord M, Allen M, Price D, Ruhl H, Springer P and Stephens R 2003 *Physical Review Letters* **91** 125004 ISSN 0031-9007 URL https://link.aps.org/doi/10.1103/PhysRevLett.91.125004

[4] Dyer G M, Bernstein A C, Cho B I, Osterholz J, Grigsby W, Dalton A, Shepherd R, Ping Y, Chen H, Widmann K and Ditmire T 2008 *Phys. Rev. Lett.* **101**(1) 015002 URL https://link.aps.org/doi/10.1103/PhysRevLett.101.015002

[5] Bulanov S V and Khoroshkov V S 2002 *Plasma Physics Reports* **28** 453–456 ISSN 1562-6938 URL http://dx.doi.org/10.1134/1.1478534

[6] Bulanov S S, Brantov A, Bychenkov V Y, Chvykov V, Kalinchenko G, Matsuoka T, Rousseau P, Reed S, Yanovsky V, Krushelnick K, Litzenberg D W and Maksimchuk A 2008 *Medical Physics* **35** 1770 (*Preprint* 0805.1766)

[7] Fuchs J, Antici P, d'Humieres E, Lefebvre E, Borghesi M, Brambrink E, Cecchetti C A, Kaluza M, Malka V, Manclossi M, Meyroneinc S, Mora P, Schreiber J, Toncian T, Pepin H and Audebert P 2006 *Nat Phys* **2** 48–54 ISSN 1745-2473 URL http://dx.doi.org/10.1038/nphys199

[8] Fritzler S, Malka V, Grillon G, Rousseau J P, Burgy F, Lefebvre E, D'Humières E, McKenna P and Ledingham K W 2003 *Applied Physics Letters* **83** 3039–3041 ISSN 00036951

[9] Ledingham K W D, McKenna P, McCanny T, Shimizu S, Yang J M, Robson L, Zweit J, Gillies J M, Bailey J, Chimon G N, Clarke R J, Neely D, Norreys P A, Collier J L, Singhal R P, Wei M S, Mangles S P D, Nilson P, Krushelnick K and Zepf M 2004 *Journal of Physics D: Applied Physics* **37** 2341–2345 ISSN 0022-3727 URL http://stacks.iop.org/0022-3727/37/i=16/a=019?key=crossref.dce227d283ba648d90e9e2adcbede670

[10] Norreys P A, Fews A P, Beg F N, Bell A R, Dangor A E, Lee P, Nelson M B, Schmidt H, Tatarakis M and Cable M D 1998 *Plasma Physics and Controlled Fusion* **40** 175 URL http://stacks.iop.org/0741-3335/40/i=2/a=001

[11] Ellison C and Fuchs J 2010 *Phys. of Plasmas* **17** 113105

[12] Morrison J T, Storm M, Chowdhury E, Akli K U, Feldman S, Willis C, Daskalova R L, Growden T, Berger P, Ditmire T, Woerkom L V and Freeman R R 2012 *Physics of Plasmas* **19** 030707 (*Preprint* http://dx.doi.org/10.1063/1.3695061) URL http://dx.doi.org/10.1063/1.3695061

[13] Alejo A, Krygier A G, Ahmed H, Morrison J T, Clarke R J, Fuchs J, Green A, Green J S, Jung D, Kleinschmidt A, Najmudin Z, Nakamura H, Norreys P, Notley M, Oliver M, Roth M, Vassura L, Zepf M, Borghesi M, Freeman R R and Kar S 2017 *Plasma Physics and Controlled Fusion* **59** 064004 URL http://stacks.iop.org/0741-3335/59/i=6/a=064004

[14] Storm M, Jiang S, Wertepny D, Orban C, Morrison J, Willis C, McCary E, Belancourt P, Snyder J, Chowdhury E, Bang W, Gaul E, Dyer G, Ditmire T, Freeman R R and Akli K 2013 *Physics of Plasmas* **20** 053106 (*Preprint* http://dx.doi.org/10.1063/1.4803648) URL http://dx.doi.org/10.1063/1.4803648

[15] Jain I P and Agarwal G 2011 *Surface Science Reports* **66** 77–172 ISSN 01675729 URL http://dx.doi.org/10.1016/j.surfrep.2010.11.001

[16] Ene A, Popescu I V and Stihi C 2009 Applications of proton-induced x-ray emission technique in materials and environmental science

[17] Hatchett S, Brown C, Cowan T, Henry E, Johnson J, Key M, Koch J, Langdon A B, Lasinski B, Lee R, Makinnon A, Pennington D, Perry M, Phillips T, Roth M, Sangster T, Singh M, Snavely R, Stoyer M, Wilks S and Yasuike K 2000 *Phys. of Plasmas* **7** 2076

[18] Gurevich A, Pariĭskaya L and Pitaevskiĭ L 1966 *Soviet Phys. JEPT* **22**

[19] Crow J E, Auer P L and Allen J E 1975 *Journal of Plasma Physics* **14** 65–76 (*Preprint* http://journals.cambridge.org/article_S0022377800025538) URL http://dx.doi.org/10.1017/S0022377800025538

[20] Mora P 2003 *Phy. Rev. Lett.* **90** 185002

[21] Link A, Freeman R R, Schumacher D W and Woerkom L D V 2011 *Physics of Plasmas* **18** 053107 (pages 8) URL http://link.aip.org/link/?PHP/18/053107/1

[22] Petrov G M, Willingale L, Davis J, Petrova T, Maksimchuk A and Krushelnick K 2010 *Physics of Plasmas* **17** 103111

[23] Borghesi M 2014 *Nuclear Instruments and Methods in Physics Research Section A: Accelerators,*

Spectrometers, Detectors and Associated Equipment **740** 6 – 9 ISSN 0168-9002 proceedings of the first European Advanced Accelerator Concepts Workshop 2013 URL http://www.sciencedirect.com/science/article/pii/S016890021301663X

[24] Kar S, Kakolee K F, Qiao B, Macchi A, Cerchez M, Doria D, Geissler M, McKenna P, Neely D, Osterholz J, Prasad R, Quinn K, Ramakrishna B, Sarri G, Willi O, Yuan X Y, Zepf M and Borghesi M 2012 *Phys. Rev. Lett.* **109**(18) 185006 URL https://link.aps.org/doi/10.1103/PhysRevLett.109.185006

[25] Macchi A, Veghini S, Liseykina T V and Pegoraro F 2010 *New Journal of Physics* **12** 045013 URL http://stacks.iop.org/1367-2630/12/i=4/a=045013

[26] Yin L, Albright B J, Hegelich B M and Fernández J C 2006 *Laser and Particle Beams* **24** 291298

[27] Flippo K, Hegelich B, Albright B, Yin L, Gautier D, Letzring S, Paffett M, Ruhl H, Schreiber J, Schulze P and Fernández J 2007 *Laser Part. Beams* **25** 3–8

[28] Hooker S M 2013 *Nature Photonics* **7** 775–782

[29] Prencipe I, Fuchs J, Pascarelli S, Schumacher D W, Stephens R B, Alexander N B, Briggs R, Büscher M, Cernaianu M O, Choukourov A, De Marco M, Erbe A, Fassbender J, Fiquet G, Fitzsimmons P, Gheorghiu C, Hund J, Huang L G, Harmand M, Hartley N J, Irman A, Kluge T, Konopkova Z, Kraft S, Kraus D, Leca V, Margarone D, Metzkes J, Nagai K, Nazarov W, Lutoslawski P, Papp D, Passoni M, Pelka A, Perin J P, Schulz J, Smid M, Spindloe C, Steinke S, Torchio R, Vass C, Wiste T, Zaffino R, Zeil K, Tschentscher T, Schramm U and Cowan T E 2017 *High Power Laser Science and Engineering* **5** e17 ISSN 2095-4719 URL https://www.cambridge.org/core/product/identifier/S2095471917000184/type/journal{_}article

[30] Sistrunk E F, Spinka T, Bayramian A, Armstrong P, Baxamusa S, Betts S, Bopp D, Buck S, Charron K, Cupal J, Demaret R, Deri R, Nicola J M D, Drouin M, Erlandson A, Fulkerson S, Gates C, Horner J, Horacek J, Jarboe J, Kasl K, Kim D, Koh E, Koubikova L, Lanning R, Lusk J, Maranville W, Marshall C, Mason D, Mazurek P, Menapace J, Miller P, Naylon J, Nissen J, Novak J, Peceli D, Rosso P, Schaffers K, Silva T, Smith D, Stanley J, Steele R, Stolz C, Telford S, Thoma J, VanBlarcom D, Weiss J, Wegner P, Rus B and Haefner C 2017 All diode-pumped, high-repetition-rate advanced petawatt laser system (hapls) *Conference on Lasers and Electro-Optics* (Optical Society of America) p STh1L.2 URL http://www.osapublishing.org/abstract.cfm?URI=CLEO_SI-2017-STh1L.2

[31] Poole P L, Willis C, Daskalova R L, George K M, Feister S, Jiang S, Snyder J, Marketon J, Schumacher D W, Akli K U, Woerkom L V, Freeman R R and Chowdhury E A 2016 *Appl. Opt.* **55** 4713–4719 URL http://ao.osa.org/abstract.cfm?URI=ao-55-17-4713

[32] McKenna P, Ledingham K W D, Spencer I, McCany T, Singhal R P, Ziener C, Foster P S, Divall E J, Hooker C J, Neely D, Langley A J, Clarke R J, Norreys P A, Krushelnick K and Clark E L 2002 *Review of Scientific Instruments* **73** 4176–4184 URL https://doi.org/10.1063/1.1516855

[33] Noaman-Ul-Haq M, Ahmed H, Sokollik T, Yu L, Liu Z, Yuan X, Yuan F, Mirzaie M, Ge X, Chen L and Zhang J 2017 *Physical Review Accelerators and Beams* **20** 1–6 ISSN 24699888

[34] Karsch S, Düsterer S, Schwoerer H, Ewald F, Habs D, Hegelich M, Pretzler G, Pukhov A, Witte K and Sauerbrey R 2003 *Phys. Rev. Lett.* **91**(1) 015001 URL https://link.aps.org/doi/10.1103/PhysRevLett.91.015001

[35] Schnürer M, Ter-Avetisyan S, Busch S, Risse E, Kalachnikov M, Sander W and Nickles P 2005 *Laser and Particle Beams* **23** 337343

[36] Sokollik T, Paasch-Colberg T, Gorling K, Eichmann U, Schnürer M, Steinke S, Nickles P V, Andreev A and Sandner W 2010 *New Journal of Physics* **12** 113013 URL http://stacks.iop.org/1367-2630/12/i=11/a=113013

[37] Hah J, Petrov G M, Nees J A, He Z H, Hammig M D, Krushelnick K and Thomas A G R 2016 *Applied Physics Letters* **109** 144102

[38] Obst L, Göde S, Rehwald M, Brack F e, Bock S, Bussmann M, Cowan T E, Curry C B, Fiuza F, Huebl A, Gauthier M, Irman A, Kazak L, Kim J B, Kluge T, Kraft S, Siebold M, Wolter S,

Ziegler T, Schramm U, Glenzer S H and Zeil K 2017 *Scientific reports* 1–9 ISSN 2045-2322

[39] Morrison J T, Chowdhury E A, Frische K D, Feister S, Ovchinnikov V M, Nees J A, Orban C, Freeman R R and Roquemore W M 2015 *Phys. Plasmas* **22** 043101 URL http://scitation.aip.org/content/aip/journal/pop/22/4/10.1063/1.4916493

[40] Orban C, Morrison J T, Chowdhury E A, Nees J A, Frische K, Feister S and Roquemore W M 2015 *Phys. Plasmas* **22** 023110 URL http://scitation.aip.org/content/aip/journal/pop/22/2/10.1063/1.4913225

[41] Feister S, Austin D R, Morrison J T, Frische K D, Orban C, Ngirmang G, Handler A, Smith J R H, Schillaci M, LaVerne J A, Chowdhury E A, Freeman R R and Roquemore W M 2017 *Optics Express* **25** 18736–18750 ISSN 1094-4087 URL https://www.osapublishing.org/abstract.cfm?uri=oe-25-16-18736

[42] Heidmann M F, Priem R J and Humphrey J C 1957 *NACA technical note* **3835** URL https://digital.library.unt.edu/ark:/67531/metadc56084/

[43] Yasuda N, Yamamura K and Mori Y H 2010 *Proc. Rol. Soc. A*

[44] Feister S, Nees J A, Morrison J T, Frische K D, Orban C, Chowdhury E A and Roquemore W M 2014 *Rev. Sci. Instrum.* **85** 11D602 URL http://scitation.aip.org/content/aip/journal/rsi/85/11/10.1063/1.4886955

[45] Seal M, Murphy N, Lombardi J and Marciniak M 2014 *Infrared physics & Technology* **67** ISSN 1350-4495 URL http://www.sciencedirect.com/science/article/pii/s1350449514001522

[46] Ziegler J, Biersack J and Ziegler M 2008 *The Stopping and Range of Ions in Matter* (Morrisville, NC: Lulu Press Co.)

[47] Bin J H, Allinger K, Khrennikov K, Karsch S, Bolton P R and Schreiber J 2017 *Scientific Reports* **7** 1–6 ISSN 20452322 URL http://dx.doi.org/10.1038/srep43548

[48] Borghesi M, Mackinnon A J, Campbell D H, Hicks D G, Kar S, Patel P K, Price D, Romagnani L, Schiavi A and Willi O 2004 *Phys. Rev. Lett.* **92**(5) 055003 URL http://link.aps.org/doi/10.1103/PhysRevLett.92.055003

[49] Welch D R, Rose D V, Clark R E, Genoni T C and Hughes T P 2004 *Computer Physics Communications* **164** 183–188

[50] Welch D R, Rose D V, Cuneo M E, Campbell R B and Mehlhorn T A 2006 *Physics of Plasmas* **13** 63105 URL https://doi.org/10.1063/1.2207587

[51] Schreiber J, Bolton P R and Parodi K 2016 *Review of Scientific Instruments* **071101** 071101 URL http://dx.doi.org/10.1063/1.4959198

[52] Palaniyappan S, DiChiara A, Chowdhury E, Falkowski A, Ongadi G, Huskins E L and Walker B C 2005 *Phys. Rev. Lett.* **94**(24) 243003 URL https://link.aps.org/doi/10.1103/PhysRevLett.94.243003

[53] Ammosov M, Delone N B and Krainov V P 1986 *Sov. Phys. JETP* **64** 1191

[54] Perelomov A and Popov V 1966 *Sov. Phys. JETP* **23** 924–934

[55] Snyder J, Ji L L and Akli K U 2016 *Physics of Plasmas* **23** 123122 (*Preprint* http://dx.doi.org/10.1063/1.4972577) URL http://dx.doi.org/10.1063/1.4972577

[56] Green J S, Carroll D C, Brenner C, Dromey B, Foster P S, Kar S, Li Y T, Markey K, McKenna P, Neely D, Robinson A P L, Streeter M J V, Tolley M, Wahlstroem C G, Xu M H and Zepf M 2010 *New Journal of Physics* **12** 085012 ISSN 13672630

[57] Jullien A, Albert O, Chériaux G, Etchepare J, Kourtev S, Minkovski N and solomon M Saltiel 2005 *J. Opt. Soc. Am. B* **22** 2635–2641 URL http://josab.osa.org/abstract.cfm?URI=josab-22-12-2635

[58] Krygier A G, Schumacher D W and Freeman R R 2014 *Physics of Plasmas* **21** 023112 (*Preprint* http://dx.doi.org/10.1063/1.4866587) URL http://dx.doi.org/10.1063/1.4866587

[59] Salehi F, Goers A J, Hine G A, Feder L, Kuk D, Miao B, Woodbury D, Kim K Y and Milchberg H M 2017 *Optics Letters* **42** 215 (*Preprint* 1610.03739)

[60] Margarone D, Klimo O, Kim I J, Prokůpek J, Limpouch J, Jeong T M, Mocek T, Pšikal J, Kim H T, Proška J, Nam K H, Štolcová L, Choi I W, Lee S K, Sung J H, Yu T J and Korn G 2012 *Phys. Rev.*

*MeV proton acceleration at kHz repetition rate from ultra-intense laser liquid interaction*17

Lett. **109**(23) 234801 URL https://link.aps.org/doi/10.1103/PhysRevLett.109.234801